Photoinduced Electron Transfer in Self-Assembled Dimers of 3-Fold Symmetric Donor−Acceptor Molecules Based on Perylene-3,4:9,10-bis(dicarboximide)

Boris Rybtchinski, Louise E. Sinks, and Michael R. Wasielewski*

Department of Chemistry and Center for Nanofabrication and Molecular Self-Assembly, Northwestern University, Evanston, Illinois 60208-3113

Received: March 12, 2004; In Final Form: July 12, 2004

The influence of π-stacking on photoinduced electron transfer in a series of donor−acceptor molecules attached to a 3-fold symmetric scaffold was studied. The donor−acceptor unit is a DEA−PDI pair (DEA = *N*,*N*-diethylaniline; PDI = perylene-3,4:9,10-bis(dicarboximide)), in which the 4-position of DEA is covalently attached to the nitrogen atom of one imide of PDI. One, two, or three DEA−PDI units are attached to the para position of one of the phenyl groups of 1,3,5-triphenylbenzene, using the other PDI imide group to form mono-, bis-, and tris(DEA−PDI). These molecules demonstrate an increasing tendency to self-assemble into π-stacked dimers in solution in the order mono(DEA−PDI) ≪ bis(DEA−PDI) < tris(DEA−PDI). Photoinduced electron transfer in both the monomers and self-assembled dimers was studied by femtosecond transient absorption spectroscopy. The charge separation (CS) and charge recombination time (CR) constants are found to be *independent* of π-stacking aptitudes, while the transient spectral features differ significantly upon dimerization. The electronic interactions imposed by π-stacking appear to change the energies of the ground, excited, and ionic states of DEA−PDI to a similar extent, which results in similar energies for CS and CR within the monomers and dimers.

Introduction

The preparation of extended molecular arrays designed to carry out energy and/or electron transfer for potential applications in organic photovoltaics is a topic of much current interest.[1−3] Significant research has been dedicated to the construction of large, covalently bonded molecular structures capable of intramolecular photoinduced charge separation.[4−11] However, as covalent synthesis is costly and time-consuming, one of the most promising approaches toward photofunctional materials is noncovalent self-assembly.[12−17] Moreover, the predefined structural relationships between the functional components of covalent donor−acceptor molecules can be used to elicit particular noncovalently assembled structures with enhanced functionality. The performance of such self-assembled photoactive structures will depend both on the photophysical properties of individual molecular components and their interactions in the self-assembled systems. Understanding these interactions is highly desirable for designing photofunctional arrays.

Highly ordered aromatic materials are important for applications in photonic and electronic devices, and much interest has been devoted to their controlled organization through intermolecular forces.[18−21] Upon formation of stacked assemblies, the photochemical properties of individual molecular components can change, since the electronic interactions intrinsic to π-stacking change the properties of the ground, excited, and radical ion pair states.[18,22] As aromatic π-stacking is primarily governed by electrostatic, dispersion, and solvophobic interactions,[23−29] aromatic chromophores possessing large π-conjugated systems with polar functional groups appear to be good building blocks for preparing stacked assemblies. An important class of such chromophores based on perylene-3,4:9,10-bis(dicarboximide) (PDI) has been successfully utilized to self-assemble functional materials by π-stacking.[19,30−39] PDI-based systems demonstrate exceptional photochemical stability, structural diversity, high fluorescence quantum yields, and low triplet yields. We recently reported a study of photoinduced electron transfer in a ZnTPP−PDI_4 donor−acceptor system (TPP = tetraphenylporphyrin), which forms π-stacked structures in solution.[40] In this system, photoinduced intramolecular electron transfer from ^{1}*ZnTPP to PDI occurs with a 3 ps time constant followed by intermolecular electron transfer between PDI molecules within the stack. In the $(ZnTPP-PDI_4)_n$ structure the photoexcited ^{1}*ZnTPP donor does not interact strongly with other neutral ZnTPP molecules nearby, whereas the PDI acceptor does. We wish to explore in more general terms how photoinduced electron transfer occurs in a system in which both the initial photoexcited state and the resultant radical ion pair product may interact with a nearby neutral donor−acceptor molecule. This is a situation that occurs in organic photovoltaic materials in the solid state.

We report here on photoinduced electron transfer in a series of molecules in which the electron donor−acceptor unit is *N*,*N*-diethylaniline−PDI (DEA−PDI), in which the 4-position of DEA is covalently attached to the nitrogen atom of one imide of PDI. One, two, or three DEA−PDI units are attached to the para position of one of the phenyl groups of 1,3,5-triphenylbenzene by using the other PDI imide group to form mono-, bis-, and tris(DEA−PDI), **4**−**6** (Figure 1). Molecules **4**−**6** demonstrate an increasing tendency to self-assemble into π-stacked dimers in solution in the order mono(DEA−PDI) ≪ bis(DEA−PDI) < tris(DEA−PDI). Photoinduced electron transfer in these compounds was studied by femtosecond transient absorption spectroscopy. Good resolution of the spectral features of the excited state and ionic intermediates facilitates identification of the states relevant to electron transfer in these π-stacking

* Address correspondence to this author. E-mail: wasielew@chem.northwestern.edu.

10.1021/jp048883u CCC: $27.50
Published on Web 08/21/2004

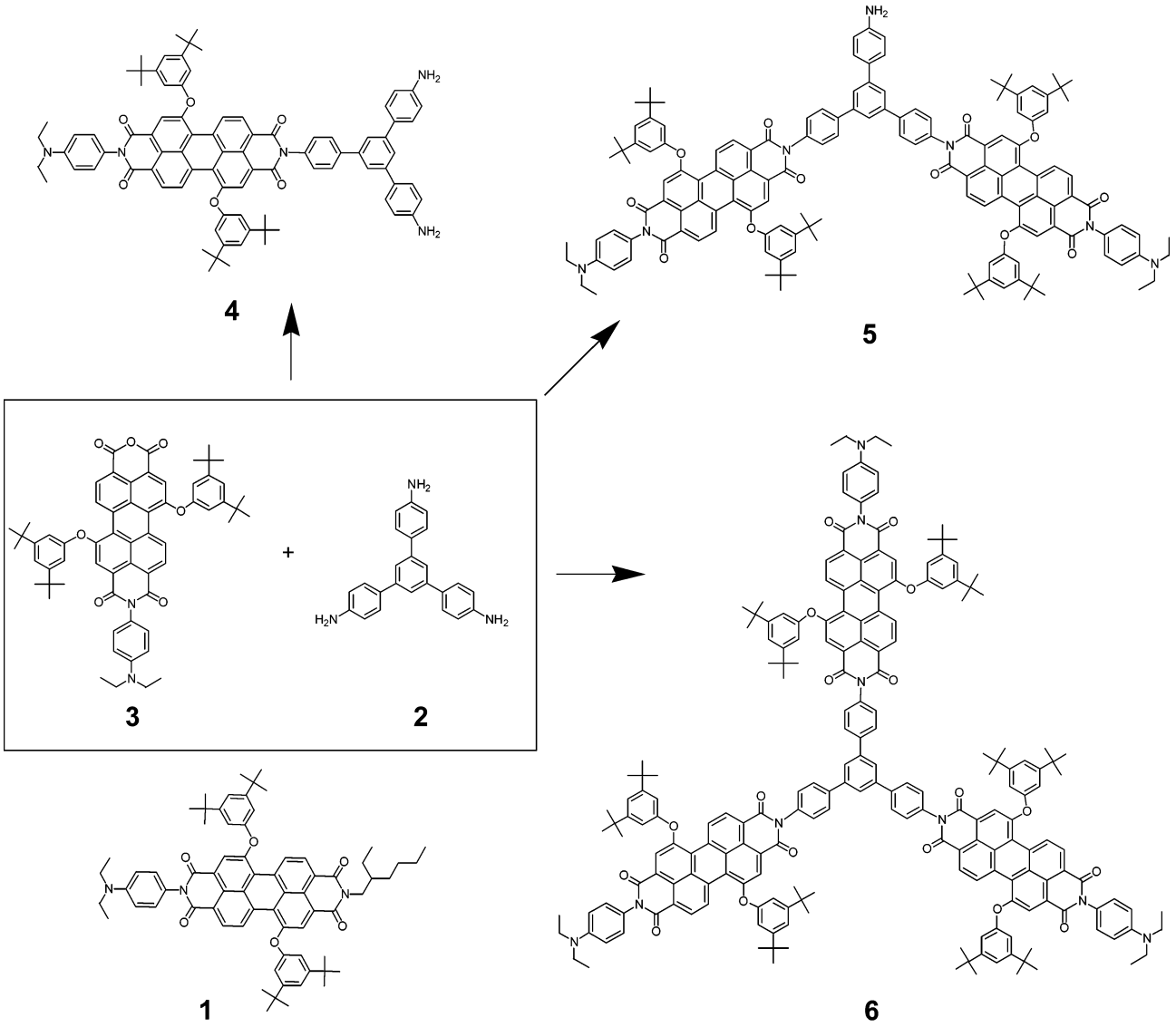

Figure 1. Structures of the molecules used in this study.

donor−acceptor systems. We find that the photoinduced charge separation (CS) and charge recombination (CR) time constants are independent of the π-stacking aptitudes, while the appearance of the spectral features differs significantly when the monomers are compared to the π-stacked dimers, providing insights into the influence of π-stacking on the electron-transfer process.

Experimental Section

Steady-State Measurements. All measurements were performed at room temperature. Proton nuclear magnetic resonance spectra were recorded on a Varian 400 spectrometer with TMS as an internal standard, and chemical shifts are given in ppm downfield from TMS. UV−vis absorption measurements were made on a Shimadzu spectrometer (UV1601). Steady-state fluorescence measurements were made on a single photon counting fluorimeter (PTI). Optical densities of solutions were kept below 0.1 in a 1-cm cuvette, and excitation/emission geometry was at right angles. All solvents were spectrophotometric grade. Dynamic light scattering (DLS) experiments were performed with a Coulter N4 Plus instrument (632.8 nm light source). Vapor pressure osmometry measurements were performed with a Knauer K-7000 osmometer and employed polystyrene (MW = 3680) as a molecular weight standard. Electrochemical measurements were performed with a CH Instruments model 660A electrochemical workstation. The solvent was methylene chloride containing 0.1 M tetra-*n*-butylammonium hexafluorophosphate ($TBAPF_6$) electrolyte. A 1.0 mm diameter platinum disk electrode, platinum wire counter electrode, and Ag/Ag_xO reference electrode were employed. Ferrocene/ferrocenium (Fc/Fc^+, 0.475 V vs SCE in CH_2Cl_2) was used as an internal reference for all measurements. All electrochemical measurements were performed under dry nitrogen atmosphere. Synthesis and characterization of the reported compounds are described in the Supporting Information.

Transient Spectroscopy. A Spectra-Physics Millenium V frequency-doubled CW $Nd:YVO_4$ laser was used to pump a home-built Ti:sapphire oscillator.[41] The 45-fs, 800-nm pulses from the oscillator were stretched to about 200 ps by using a four-pass, reflective, single-grating pulse stretcher and are used to seed a homemade regenerative amplifier,[42] which includes a Clark-MXR Pockels cell, and is pumped at a 1 kHz repetition rate by a Quantronix 527DP frequency-doubled Nd:YLF laser (5.2 mJ/pulse). The amplified Ti:sapphire pulse (0.7 mJ/pulse) is recompressed to approximately 80 fs by a four-pass, reflective, single grating compressor. The pulse energy after compression is 440 μJ/pulse. Two 5% reflective beam splitters are placed in the output path to generate two 800-nm beams for white light

generation. The remaining 800-nm light is frequency doubled by using a 1-mm-type I LBO crystal to give 400-nm, 80-fs, 80-μJ pulses.[42] The 800-nm light from the first 5% beam splitter is passed though a waveplate−polarizer pair to control its intensity, and a few microjoules are focused into a 1-mm sapphire disk to generate white light continuum probe pulses. All-reflective optics were used both to focus the 800-nm pulse into the sapphire and recollimate the white light output, thus limiting the chirp on the white light pulse to <200 fs. The 800-nm light from the second 5% beam splitter was used to create a second white light continuum by focusing the 800-nm pulse into a 2-mm sapphire disk, using a 100 mm focal length (f.l.) lens. This white light was used to seed the first stage of a two-stage OPA, which was previously described.[43,44] The first stage contains a Type II BBO crystal, which is pumped with about 20−25 μJ of 400-nm light focused into the crystal with a 300 mm f.l. lens. After removal of the IR idler beam and residual 400-nm pump, the first stage produced transform-limited pulses having ~0.5 μJ/pulse from 460 to 750 nm. This light is then focused into the Type I BBO of the second stage of the OPA with a 75 mm f.l. lens. The second stage amplifies the first stage light upon overlap with the remaining 55−60 μJ of 400 nm pump light. The final amplified pulse is ~10 μJ/pulse after filtering out the residual 400-nm and IR idler light. For experiments with 400-nm excitation, the white light input to the OPA was turned off by blocking the sapphire with a beam block. The blue light through the first stage OPA was similarly turned off, so that the 400-nm pump traveled only through the second stage of the OPA. Energy levels were sufficiently low that no continuum generation was observed in the BBO I crystal. The optical path for the probe beams, 400 nm or OPA, and the chopping scheme used to perform pump−probe experiments are described by Lukas et al.[42]

The instrument was outfitted with a CCD array detector (Ocean Optics PC2000) for simultaneous collection of spectral and kinetic data.[45] The total instrument response function for the pump−probe experiments was 130 fs. Typically 5 s of averaging were needed to obtain the transient spectrum at a given delay time. Cuvettes with a 2 mm path length were used and the samples were irradiated with 0.5−1.0 μJ per pulse focused to a 200-μm spot. The optical density at λ_{max} was typically 0.4−0.8. Kinetic analyses were performed at several wavelengths by using a Levenberg−Marquardt nonlinear least-squares fit to a general sum-of-exponentials function with an added Gaussian to account for the finite instrument response.

Results and Discussion

Synthesis and Self-Assembly. It has been shown that photoinduced electron transfer occurs readily from aromatic amines attached to PDI molecules.[46] In light of this observation, compounds **1**−**6** (Figure 1) were synthesized and characterized by mass spectrometry, ^{1}H NMR, and UV−vis spectroscopy (see the Supporting Information). Model compound **1** was synthesized to characterize the photoinduced electron-transfer reaction within a single DEA−PDI molecule. The 1,3,5-tris(4-aminophenyl)benzene scaffold, **2**, was synthesized by using a literature procedure,[47] and allows the introduction of a variable number of DEA−PDI units. Compound **2** was condensed with *N*′-(*N*,*N*-diethylaminophenyl)perylene-3,4-dicarboximide-9,10-dicarboxyanhydride, **3**, to yield mono-, bis-, and tris(DEA−PDI), **4**, **5**, and **6**, respectively. In the absence of an electron donor, the fluorescence quantum yield of ^{1}*PDI is nearly unity; however, the fluorescence yields of **1** and **4**−**6** are strongly quenched (φ_F < 0.001) even in relatively nonpolar solvents such as toluene, suggesting that a fast and efficient electron-transfer reaction takes place. This was confirmed by transient absorption studies (see below).

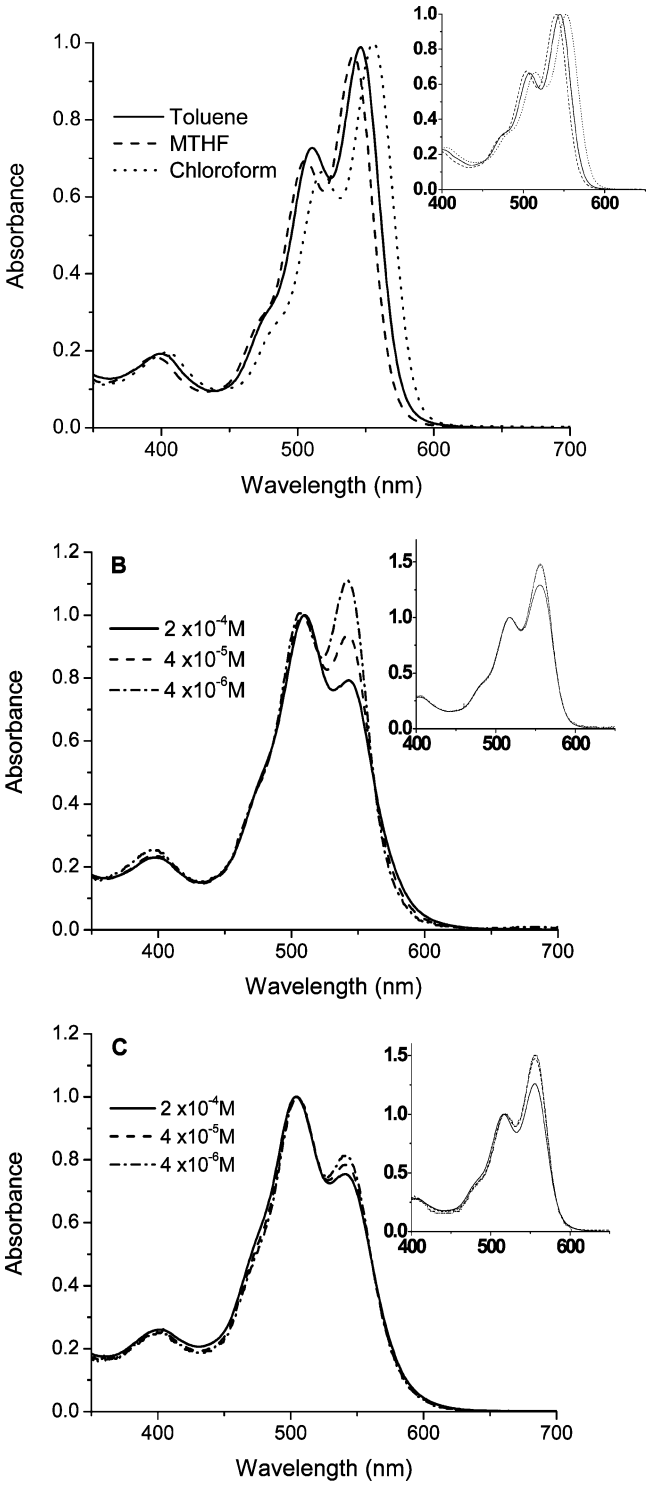

Figure 2. Normalized UV−vis spectra of (A) **4** and **1** (inset) in toluene, MTHF, and chloroform, (B) **5** in MTHF and $CHCl_3$ (inset), and (C) **6** in MTHF and chloroform (inset).

Elucidation of the π-stacked aggregate structures in solution presents a significant challenge. Yet, PDI-based systems have the advantage that π-stacking results in distinctive UV−vis spectral changes due principally to exciton coupling between the transition dipoles of adjacent chromophores.[48] For example, exciton interactions between the PDI chromophores in a J-aggregate (slipped stack geometry) show red-shifted absorption spectra, while the corresponding H-aggregates (cofacial geom-

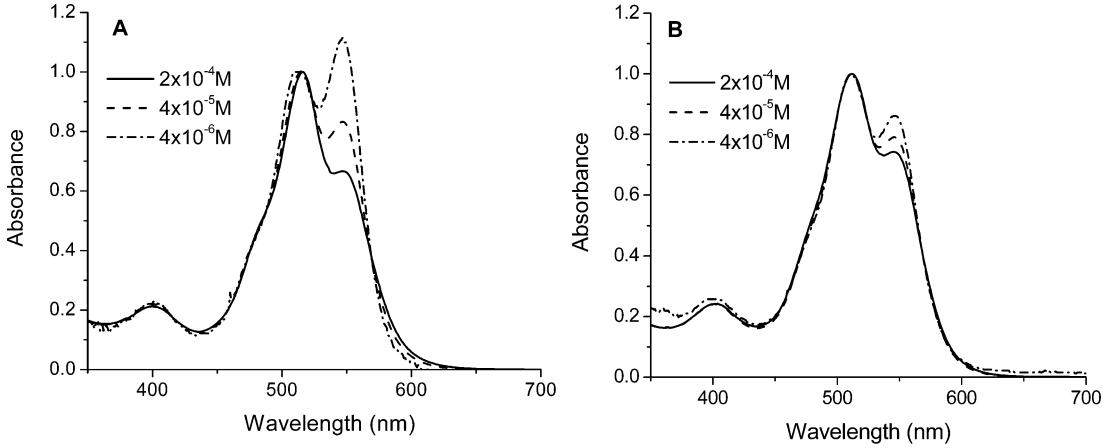

Figure 3. Normalized UV−vis spectra of (A) **5** in toluene and (B) **6** in toluene.

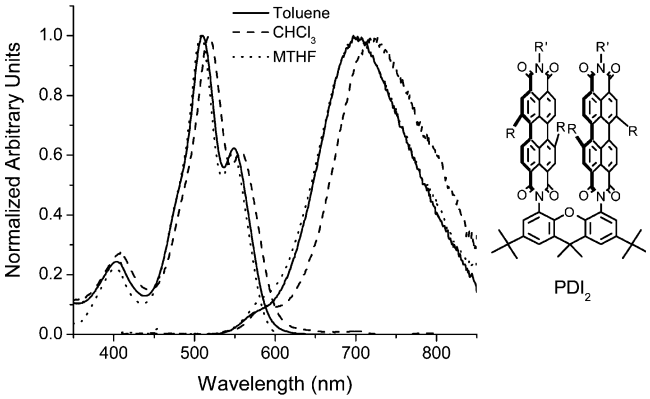

Figure 4. Normalized UV−vis and fluorescence spectra of PDI_2 (R = 3,5-di-*tert*-butylphenoxy; R′ = 2-ethylhexyl).

etry) demonstrate blue-shifted spectra.[48] In general, the blue shift in H-aggregates results in an enhanced 0−1 vibronic band in cofacially stacked PDI compared to that of nonstacked PDI molecules due to strong vibronic coupling.[35,49,50] These spectral changes provide a useful tool for roughly determining the PDI stacking geometry in solution.[30,36,37,51]

UV−vis spectra show that **1** and **4** do not aggregate in $CHCl_3$, toluene, and MTHF (Figure 2A). On the other hand, bis(DEA−PDI), **5**, demonstrates a moderate degree of H-aggregate formation, i.e., some enhancement of the 0−1 vibronic band, in toluene and MTHF, while in $CHCl_3$ its UV−vis absorption is characteristic of a disaggregated species (Figures 2B and Figure 3A). On the other hand, tris(DEA−PDI), **6**, shows a strong tendency to self-assemble into H-aggregates in both toluene and MTHF as denoted by the strong enhancement of the 0−1 vibronic band (Figures 2C and Figure 3B), while in $CHCl_3$ **6** shows only a small enhancement of the 0−1 vibronic band suggesting that it is largely disaggregated (Figure 2C, inset). Remarkably, the UV−vis spectra of **6** in toluene and MTHF show that it remains largely aggregated at low concentrations ($\sim 10^{-6}$ M). Compound **6** also exhibits significant aggregation in dichloromethane solutions at concentrations above 10^{-5} M as indicated by UV−vis spectroscopy. For comparison, Figure 4 shows the UV−vis absorption and fluorescence emission spectra from the cofacial PDI_2 reference dimer that we reported earlier.[40] In this dimer the orientation of the transition moments of the two PDI chromophores is forced by the xanthene spacer to adopt a parallel orientation leading to essentially solvent-independent blue-shifted spectra.

The molecular weight of the aggregate of **6** in toluene at 5×10^{-3} to 1×10^{-2} M measured by vapor pressure osmometry (VPO) is ~6 kD. Since the molecule weight of the monomer is 3136.5, the VPO data indicate that the aggregate is a dimer. In addition, we performed dynamic light scattering (DLS) experiments on solutions of **6** as high as 10^{-3} M in toluene. No significant scattering signal was observed, indicating that the aggregate size (mean particle size, assuming a spherical particle model) is below the 3 nm detection limit of the instrument. Thus based on UV−vis, VPO and DLS data, **6** self-assembles into a π-stacked dimer, in which the orientation of the PDI chromophores should be approximately cofacial. The formation of significant concentrations of larger aggregates of **6** is not supported by our measurements. Compound **5** is most likely a dynamic mixture of monomer and dimer, as indicated by UV−vis spectra (Figures 2 and 3).

^{1}H NMR spectra of the aromatic protons within π-stacked PDI molecules show characteristic upfield ring current shifts,[37,50] and are therefore potentially useful for determining the structures of these stacked systems. ^{1}H NMR spectra of **1**, **4**, and **5** in $CDCl_3$ are characteristic of monomers. In contrast, ^{1}H NMR resonances of **6** in $CDCl_3$ are severely broadened in the 10^{-4} to 10^{-2} M concentration range, which is most probably due to a dynamic equilibrium between monomers and dimers. Notably, the aromatic PDI resonances of **6** in toluene-d_8 are significantly less broadened than those observed in $CDCl_3$, and are shifted upfield relative to those of monomeric **4** by approximately $\Delta\delta = 0.1-0.2$ ppm indicating π-stacking of **6** (Figure 5).[37,50] Thus, the dimerization equilibrium in toluene, which appears to be slow on the NMR time scale, is shifted strongly toward the dimer. This is in agreement with the UV−vis data showing that **6** is aggregated and that **4** and **1** are disaggregated at this concentration. Moreover, in the concentration range 2×10^{-4} to 2×10^{-3} M (toluene-d_8), the chemical shifts and the shape of the PDI aromatic resonances of **6** are *independent of concentration*, which lends further support to dimer formation (Figure S1, Supporting Information).[52,53]

Our NMR, VPO, and UV−vis data suggest that all PDI units of **6** are involved in cofacial π-stacking interactions, which implies a dimer geometry where two molecules of **6** are positioned on top of one another. In light of these observations we performed a force field optimization of the dimer structure, using a roughly cofacial dimer geometry as the starting point for the calculation. Figure 6 shows the energy-minimized dimer structure calculated by using the MM+ force field.[54] All three pairs of stacked PDI molecules adopt similar conformations, and the calculated PDI interplanar distances average to ~3.5 Å. Although molecular mechanics calculations employ a high degree of approximation, they have been shown to give a

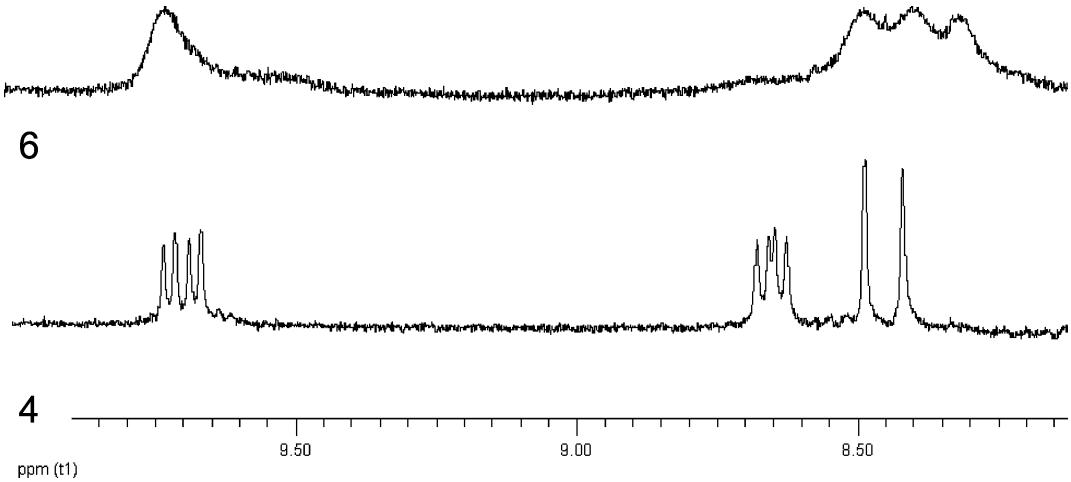

Figure 5. ^{1}H NMR spectrum of the PDI aromatic ring resonances of **4** and **6** at 2×10^{-3} M in toluene-d_8.

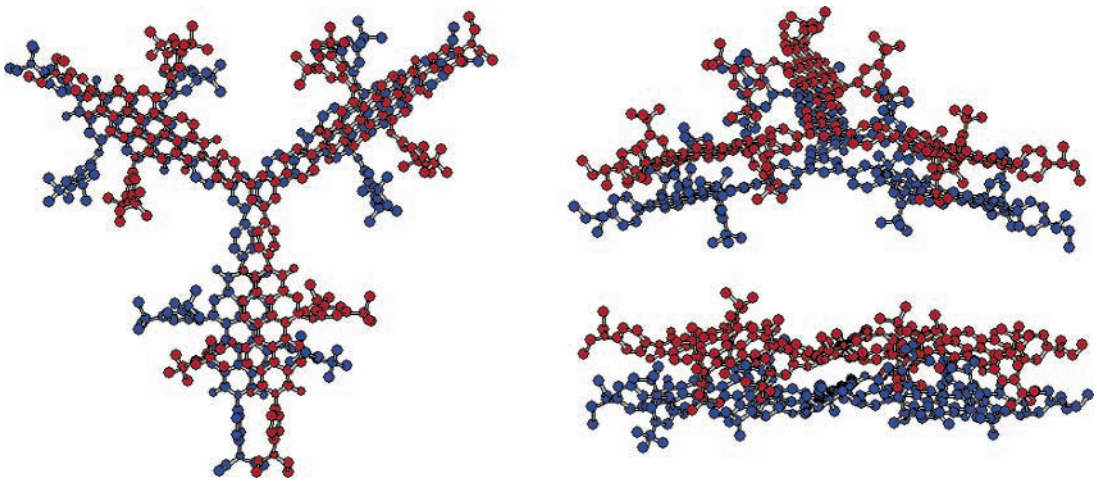

Figure 6. MM+ energy-minimized structure of the dimer of **6**, with views along the *x*, *y*, and *z* axes.

TABLE 1: One-Electron Redox Potentials ($E_{1/2}^{RED}$, $E_{1/2}^{OX}$), Excitation Energy (E_{S1}), and Free Energies of Charge Separation (ΔG_{CS}) and Charge Recombination (ΔG_{CR}) for 1 and 6[a]

	$E_{1/2}^{RED}$ (V)	$E_{1/2}^{OX}$ (V)	E_{S1} (eV)	ΔG_{CS} (eV)		ΔG_{CR} (eV)	
				MTHF	toluene	MTHF	toluene
1	−0.70	0.97	2.21	−0.67	−0.14	−1.58	−2.11
6	−0.68	0.84	ca. 1.9	ca. −0.5	ca. 0.0	ca. −1.4	ca. −1.9

[a]Compound **6** was aggregated at the conditions of measurement, as verified by UV−vis spectroscopy. See the Supporting Information for cyclic voltammograms.

satisfactory estimate of the stacking interactions in many systems.[55−58] Our calculated structure of the π-stacked dimer of **6** is consistent with our experimental results.

Electron Transfer. To estimate the energetics of charge separation in the monomer vs the dimer cyclic voltammetry (CV) in dichloromethane was performed on compounds **1** and **6**. Compound **6** is dimeric under the conditions of the CV measurement, as indicated by UV−vis spectroscopy. The CVs of both **1** and **6** show reversible one- and two-electron reductions of PDI[40] and reversible oxidation of DEA[59] (Table 1, see also Figure S2 in the Supporting Information). The energy of the lowest excited singlet state of monomeric PDI, $E_{S1} = 2.21$ eV, is obtained from the average of the energies of its absorption maximum at 2.27 eV (548 nm) and emission maximum at 2.16 eV (575 nm) (Table 1).[40,60] Since the UV−vis absorption of the upper exciton band of dimeric **6** occurs at 2.44 eV (511 nm), the lower disallowed absorption should be 1.98 eV (~630 nm). As the fluorescence emission from all the DEA−PDI derivatives is strongly quenched, we will rely on the fluorescence emission from the PDI_2 reference dimer, which has absorption spectra nearly identical with those of dimeric **6**, to estimate the excited-state energies of the PDI excited states in dimeric **6**. The fluorescence maximum of PDI_2 occurs at 700 nm with $\varphi_F = 0.15$ (Figure 4), and is strongly red-shifted relative to the 575-nm emission maximum of the PDI monomer. The presence of this relatively strong emission implies that it does

TABLE 2: Time Constants for Photoinduced Charge Separation and Thermal Radical Ion Pair Decay for the Indicated Compounds[a]

	CS time constant (ps)		CR time constant (ps)	
compd	toluene	MTHF	toluene	MTHF
1	0.7 ± 0.1	0.8 ± 0.3	16 ± 3	3.4 ± 0.5
4	0.8 ± 0.1	1.5 ± 0.5	16 ± 3	4.3 ± 1.0
5	0.7 ± 0.1	0.5 ± 0.1	20 ± 2	5.1 ± 1.2
6	0.6 ± 0.1	0.7 ± 0.2	16 ± 2	4.5 ± 0.2

[a] The error bars are 1 standard deviation. These time constants were determined at 740 nm.

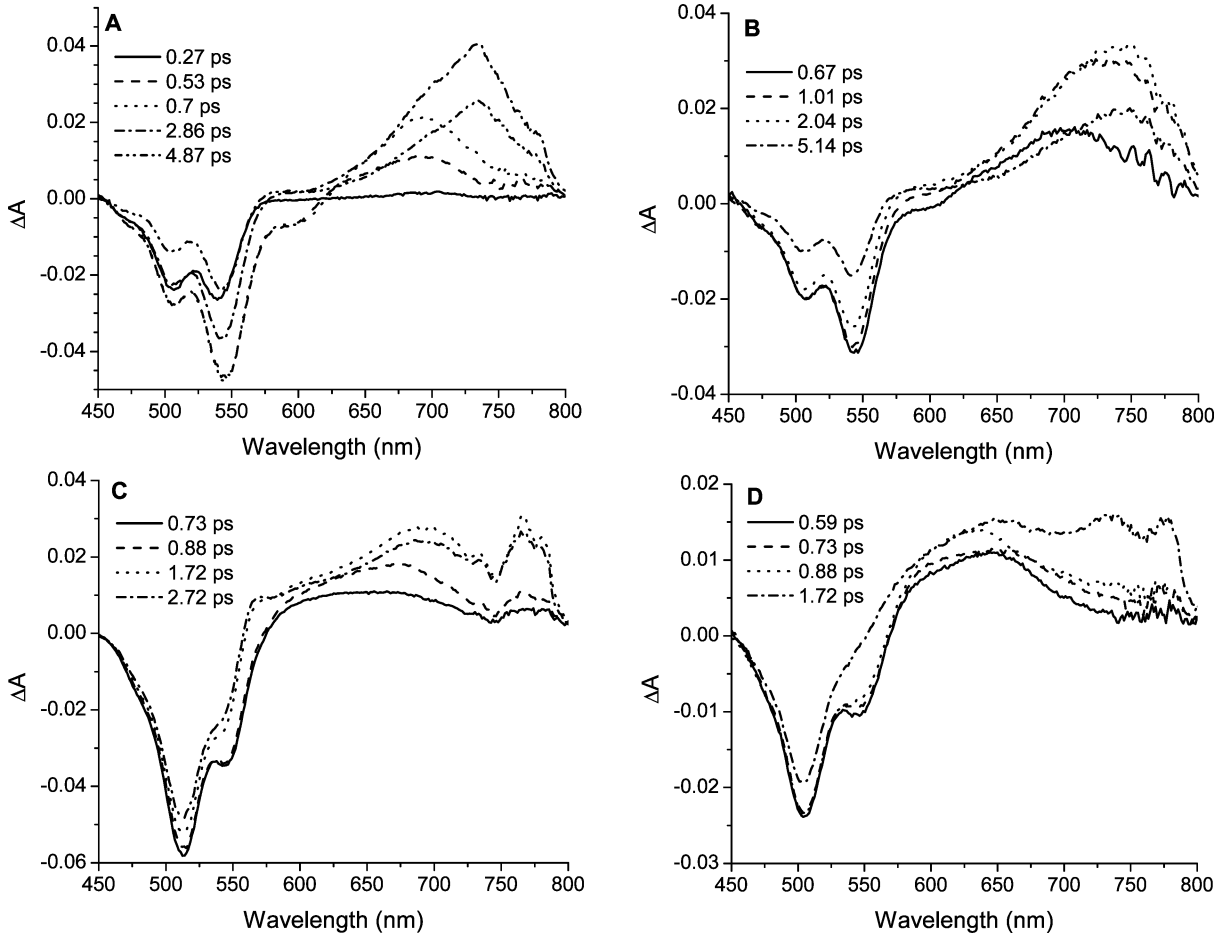

Figure 7. Femtosecond transient absorption spectra in MTHF following a 400 nm laser flash: (A) **1**, (B) **4**, (C) **5**, and (D) **6**.

not originate from the strongly disallowed transition[48] from the lower exciton state to the ground state. It is due to an excimer-like state that is below the energy of the nearby lower exciton state of the dimer. The energies of the lower exciton states of both PDI_2 and dimeric **6** are 1.98 eV, while the emission from the excimer-like state of PDI_2 occurs at 1.77 eV. Since the emission occurs exclusively from the excimer-like state, these two energies bracket the energy of the excimer-like state, and thus we estimate that the energy of the excimer-like state is ~1.9 eV. The free energies for the photoinduced charge separation (ΔG_{CS}) and charge recombination (ΔG_{CR}) reactions are calculated by using the Weller equation[61] (see the Supporting Information for details). It should be noted that the oxidation potential of the DEA donor is lower in dimeric **6** ($E_{1/2}^{OX} = 0.84$ V) than in monomeric **1** ($E_{1/2}^{OX} = 0.97$ V), indicating that the DEA radical cation is more stable in the dimer than in the monomer. Using this approach the data shown in Table 1 indicate that both ΔG_{CS} and ΔG_{CR} change by no more than 0.2 eV between monomeric **1** and dimeric **6**. These calculations of free energies are at best an estimate because having the charges delocalized between dimeric donors and/or acceptors will also change the solvation, ionic radii, and perhaps the radical ion pair distances as well.

Femtosecond transient absorption studies with 400-nm pulses were used to investigate the photochemistry of stacked arrays of **5** and **6** as well as their nonstacked counterparts **1** and **4.** The transient absorption spectra of **1** and **4**−**6** in MTHF and toluene reveal that ultrafast electron transfer from DEA to ^{1}*PDI results in formation of $PDI^{-\bullet}$ (Table 2, Figures 7 and 8).[40,62] The kinetics show that the time constants for the decay of $PDI^{-\bullet}$ in all compounds measured at ~700 nm match the recovery of the ground-state bleaches at 511 and 550 nm, indicating that charge recombination produces the ground state. Additionally, compounds **1**, **4**, and **6** in toluene were excited at 550 nm to verify that electron transfer did not occur from the S_2 (400 nm) or upper exciton state (511 nm). Both the spectral and kinetic data were the same within experimental error for samples excited at 400 or 550 nm. The data obtained with 400-nm excitation are shown in Figures 7 and 8. In **6** we do not observe spectral changes using either 400- or 550-nm excitation at times greater than the 130 fs instrument response that can be attributed to formation of the excimer-like state from either the upper or lower exciton states (Figure 8D as well as Figure S3 in the Supporting Information). It appears that the first discernible process in the dimers is CS from the excimer-like state. We do not observe a spectral feature due to $DEA^{+\bullet}$ because this radical cation has a weak extinction coefficient compared to those of the transient PDI intermediates.[40,63] However, it is important to note that good resolution of the ^{1}*PDI and $PDI^{-\bullet}$ spectral features was achieved, and very similar spectra were observed in both MTHF and toluene. Remarkably, we observe very similar time constants for CS and CR in all our compounds regardless of their aggregation state: in toluene $\tau_{CS} = 0.6-0.8$ ps and $\tau_{CR} = 16-20$ ps, while in MTHF $\tau_{CS} = 0.5-1.5$ ps and $\tau_{CR} = 3.4-5.1$ ps for compounds **1** and **4**−**6** (Table 2). This occurs despite the fact that dimeric **5** and **6** exhibit severely broadened and blue-shifted transient absorption features that are dramatically different from the appearance of these features in **1** and **4** (Figures 7 and 8). For example, the time evolution of the transient features of **1** in MTHF (Figure 7A) shows that the absorption due to ^{1}*PDI at 693 nm observed at 0.7 ps is replaced at 3 ps with a sharper feature at 734 nm characteristic of $PDI^{-\bullet}$.[62]

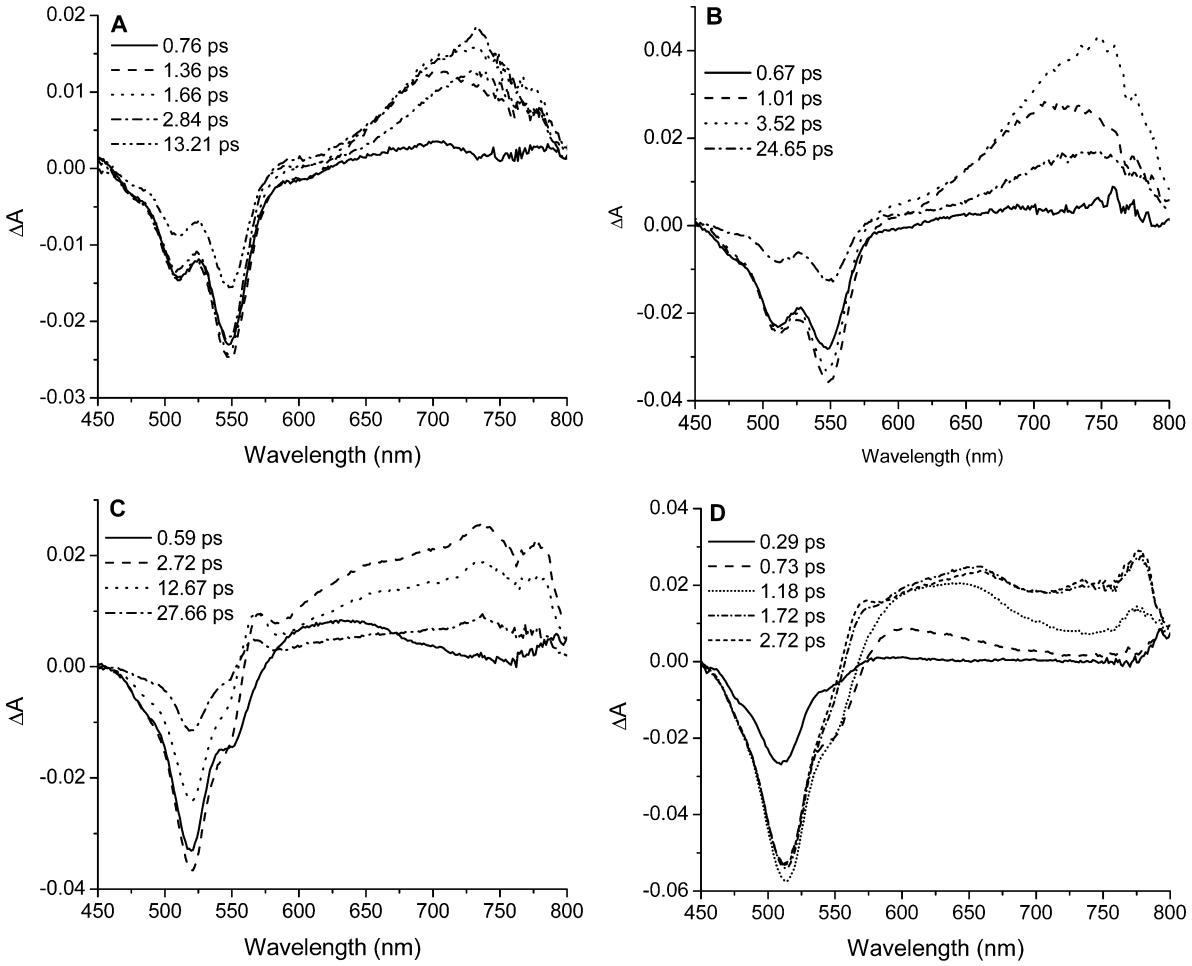

Figure 8. Femtosecond transient absorption spectra in toluene following a 400 nm laser flash: (A) **1**, (B) **4**, (C) **5**, and (D) **6**.

The ^{1}*PDI and PDI$^{-\bullet}$ spectral features of **4** are slightly broadened, but peak at nearly the same wavelengths as those of **1**, 700 nm for ^{1}*PDI and 740 nm for PDI$^{-\bullet}$ (Figure 7B). Significantly, both the ^{1}*PDI and PDI$^{-\bullet}$ peaks in **5** and **6** in both MTHF and toluene (Figures 7C,D and 8C,D, respectively) are blue shifted in comparison to those of **1** and **4** (Figures 7A,B and 8A,B). For example, in MTHF, the ^{1}*PDI feature shifts to 675 nm in **5** and about 645 nm in **6**, whereas the PDI$^{-\bullet}$ feature displays peaks at 693 and 767 nm in **5** and at 651, 735, and 776 nm in **6**. Considerable spectral broadening of these features, especially those of PDI$^{-\bullet}$, also occurs in both **5** and **6**. The degree of broadening corresponds well to the tendency to self-assemble: **6** > **5** ≫ **4**, **1**. The spectral features of compound **5** are intermediate between those of **4** and **6**, in agreement with its aggregation behavior (monomer−dimer mixture). The broad appearance of PDI$^{-\bullet}$ peaks in the spectra of the dimers are consistent with those observed in covalently linked cofacial PDI dimers and in (ZnTPP−PDI$_4$)$_n$ aggregates.[40]

Monomer vs Dimer Energetics. To analyze electron transfer in π-stacked arrays, all photochemically relevant interactions imposed by aggregation must be considered: (a) ground-state interactions; (b) excited-state interactions (exciton coupling and excimer formation); and (c) the interaction of the radical ions with their neutral neighbors. Our system allows observation of all these interactions, since they result in distinct photophysical signatures. As a consequence, both steady state and transient absorption spectra of the dimers are very different from those of the monomers.

Ground state π-stacking interactions in dimeric **6** are indicated by enhancement of the 0−1 vibronic band in the UV−vis spectrum, compared to the spectrum of monomeric PDI in the case of **1** and **4**. Ground state π-stacking interactions have been extensively studied in organic crystals, where they are known to lower the energy of the HOMO (Figure 9).[18]

A comparison of the ^{1}*PDI and PDI$^{-\bullet}$ spectral features in the dimers vs the monomers clearly demonstrates the influence of π-stacking on the states associated with electron transfer. Stacking changes the energy of the initial excited state from which CS occurs primarily due to contributions from both exciton splitting and the formation of an excimer-like state (Figure 9).[18] Ground state cofacial stacking is known to promote excimer formation by greatly enhanced interaction of the initially localized excited state with the ground state of a nearby molecule.[18,64] Thus, the fact that PDI is a dimer in the ground state facilitates subpicosecond formation of the excimer-like state, which results in the appearance of the blue-shifted, broad ^{1}*PDI absorption in **6** (Figures 7D and 8D). Such a blue-shifted broad transient feature is characteristic of an excimer state.[65,66]

While it may seem that since CS occurs from the excimer-like state, ΔG_{CS} (and, therefore τ_{CS}) should be different for the dimer vs the monomer, we observe that the energetics of the ion pair are also changed, due to the interactions of DEA$^{+\bullet}$−PDI$^{-\bullet}$ with an adjacent neutral DEA−PDI in the stacked dimer. In turn, it is possible that variations in the CR rates will occur as a result of stabilization of the radical ion pair in the stacked dimer. It has been shown that radical cations[67] and radical anions[68] interact in solution with their neutral counterparts forming neutral molecule−radical ion dimers (π-mers). In fact, our redox potential measurements demonstrate that DEA$^{+\bullet}$ is stabilized to a greater extent in the aggregated compounds

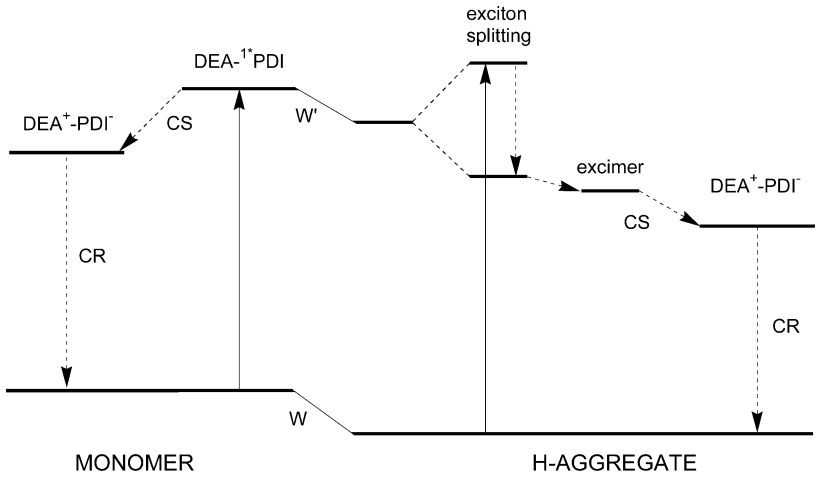

Figure 9. Energy level diagram for a DEA−PDI monomer and cofacial DEA−PDI dimer.

(compare $E_{1/2}^{OX}$ for **1** and **6**, Table 1), due to the interaction of this cation with its neutral neighbor (DEA/DEA$^{+\bullet}$ interaction) in the π-stacked dimer. Interestingly, no significant difference in $E_{1/2}^{RED}$ of PDI was observed, while the transient spectral feature of PDI$^{-\bullet}$ changed significantly as a function of dimerization, indicating PDI/PDI^{-} interaction. It should be noted, however, that the properties of a covalently linked radical ion pair formed in a photoinduced electron transfer can differ from those of singly reduced or oxidized species in electrochemical experiments.

On the whole, it appears that all the DEA−PDI, DEA−^{1}*PDI, and DEA$^{+\bullet}$−PDI$^{-\bullet}$ energy levels within the dimers of **6** are stabilized relative to their monomeric counterparts **1** and **4** (Figure 9), resulting in the energy gaps for **6** being similar to those for **1**. Consequently, the overall CS and CR rates should not change much in agreement with our experimental data (Table 2).

It should be noted that solvent interactions with the dimer of **6** may differ significantly from those in monomers **1** or **4**, and can also contribute to the observed phenomena. Specific solvent−solute interactions almost certainly influence the DEA−PDI, DEA−^{1}*PDI, and DEA$^{+\bullet}$−PDI$^{-\bullet}$ energy levels in a manner different for the monomers vs dimers. Overall, the interactions between the individual molecules in the dimers and specific interactions with the solvent should be considered in order to develop an adequate quantitative picture of the electron transfer in stacked donor−acceptor molecules. Research aimed at developing a satisfactory quantitative model for electron transfer in soluble π-stacked aggregates is currently underway in our laboratory.

Conclusions

The self-assembling DEA−PDI systems described here allow us to observe all the major photochemical consequences of π-stacking in solution that are relevant to electron transfer: (a) ground-state interactions, (b) formation of excimer-like excited states, and (c) radical ion pair state interactions. These interactions appear to change the CS and CR energetics in the same direction by similar amounts. As the basic building block of any photoinduced electron-transfer system is a donor−acceptor dyad, an understanding of the influence of stacking between two such dyads is an important prerequisite for the utilization of large molecular arrays such as **6** in photofunctional materials. Our study demonstrates that the noncovalent dimerization of two photofunctional donor−acceptor units leads to a variety of photophysical changes in comparison to the monomers. However, the overall outcome of these changes is somewhat surprising, namely that electron-transfer rates in the dyad units of the stacked dimer are very similar to those of the monomeric dyad. This phenomenon, if it proves to be general, may simplify the design of photofunctional materials for organic photovoltaics based on π-stacking between donor−acceptor moieties.

Acknowledgment. This work was supported by the Office of Naval Research (N00014-02-1-0381). We thank Dr. A. E. Ribbe (Purdue Laboratory for Chemical Nanotechnology) for performing VPO measurements, and Prof. P. B. Messersmith (Department of Biomedical Engineering, Northwestern University) for DLS instrument time. We also wish to thank Dr. M. J. Tauber and Ms. E. A. Weiss for valuable discussions, Mr. B. Jones for technical assistance, and Mr. J. Giaimo for providing the data on PDI_2 on the xanthene scaffold.

Supporting Information Available: Details regarding the synthesis and characterization of the molecules used in this study, electrochemical data, additional transient absorption data, and calculations of ΔG_{CS} and ΔG_{CR}. This material is available free of charge via the Internet at http://pubs.acs.org.

References and Notes

(1) Balzani, V.; Scandola, F. *Supramolecular photochemistry*; Ellis Horwood: New York, 1991.
(2) Turro, N. J. *J. Photochem. Photobiol. A* **1996**, *100*, 53−56.
(3) Armaroli, N. *Photochem. Photobiol. Sci.* **2003**, *2*, 73−87.
(4) Closs, G. L.; Miller, J. R. *Science* **1988**, *240*, 440−447.
(5) Paddon-Row, M. *Aust. J. Chem.* **2003**, *56*, 729−748.
(6) Meyer, T. J. *Acc. Chem. Res.* **1989**, *22*, 163−170.
(7) Wasielewski, M. R. *Chem. Rev.* **1992**, *92*, 435−461.
(8) Gust, D.; Moore, T. A.; Moore, A. L. *Acc. Chem. Res.* **2001**, *34*, 40−48.
(9) Holten, D.; Bocian, D. F.; Lindsey, J. S. *Acc. Chem. Res.* **2002**, *35*, 57−69.
(10) Aratani, N.; Osuka, A.; Chob, H. S.; Kim, D. *J. Photochem. Photobiol. C* **2002**, *3*, 25−52.
(11) Imahori, H.; Mori, Y.; Matano, Y. *J. Photochem. Photobiol. C* **2003**, *4*, 51−83.
(12) Shimomura, M.; Karthaus, O.; Ijiro, K. *Synth Met.* **1996**, *81*, 251−257.
(13) Dinolfo, P. H.; Hupp, J. T. *Chem. Mater.* **2001**, *13*, 3113−3125.
(14) Reinhoudt, D. N.; Crego-Calama, M. *Science* **2002**, *295*, 2403−2407.
(15) Kaschak, D. M.; Johnson, S. A.; Waraksa, C. C.; Pogue, J.; Mallouk, T. E. *Coord. Chem. Rev.* **1999**, *185*−*186*, 403−416.
(16) Kobuke, Y.; Ogawa, K. *Bull. Chem. Soc. Jpn.* **2003**, *76*, 689−708.
(17) Hwang, I.-W.; Cho, H. S.; Jeong, D. H.; Kim, D.; Tsuda, A.; Nakamura, T.; Osuka, A. *J. Phys. Chem. B* **2003**, *107*, 9977−9988.

(18) Pope, M.; Swenberg, C. E. *Electronic Processes in Organic Crystals and Polymers*, 2nd ed.; Oxford University Press: New York, 1999.
(19) Würthner, F. *Angew. Chem., Int. Ed.* **2001**, *40*, 1037−1039.
(20) Anthony, J. E.; Eaton, D. L.; Parkin, S. R. *Org. Lett.* **2002**, *4*, 15−18.
(21) Sheraw, C. D.; Jackson, T. N.; Eaton, D. L.; Anthony, J. E. *Adv. Mater.* **2003**, *15*, 2009−2011.
(22) Kazmaier, P. M.; Hoffmann, R. H. *J. Am. Chem. Soc.* **1994**, *116*, 9684−9691.
(23) Hunter, C. A.; Sanders, J. K. M. *J. Am. Chem. Soc.* **1990**, *112*, 5525−5534.
(24) Hunter, C. A.; Lawson, K. R.; Perkins, J.; Urch, C. J. *J. Chem. Soc., Perkin. Trans.* **2001**, 651−669.
(25) Waters, M. L. *Curr. Opin. Chem. Biol.* **2002**, *6*, 736−741.
(26) Zhao, D.; Moore, J. S. *Chem. Commun.* **2003**, 807−818.
(27) Sui, G.; Orbulescu, J.; Mabrouki, M.; Leblanc, R. M.; Liu, S.; Gregg, B. A. *ChemPhysChem* **2002**, *12*, 1041−1044.
(28) Sui, G.; Orbulescu, J.; Mabrouki, M.; Micic, M.; Leblanc, R. M.; Liu, S.; Cormier, R. A.; Gregg, B. A. *J. Phys. Chem. B* **2002**, *106*, 9335−9340.
(29) Liu, S.-G.; Sui, G.; Cormier, R. A.; Leblanc, R. M.; Gregg, B. A. *J. Phys. Chem. B* **2002**, *106*, 1307−1315.
(30) Würthner, F.; Thalacker, C.; Sautter, A.; Schartel, W.; Ibach, W.; Hollricher, O. *Chem. Eur. J.* **2000**, *6*, 3871−3886.
(31) Sautter, A.; Thalacker, C.; Heise, B.; Würthner, F. *Proc. Natl. Acad. Sci. U.S.A.* **2002**, *99*, 4993−4996.
(32) Schmidt-Mende, L.; Fechtenkotter, A.; Müllen, K.; Moons, E.; Friend, R. H.; MacKenzie, J. D. *Science* **2001**, *293*, 1119−1122.
(33) Schenning, A. P. H. J.; Herrikhuyzen, J. v.; Jonkheijm, P.; Chen, Z.; Würthner, F.; Meijer, E. W. *J. Am. Chem. Soc.* **2002**, *124*, 10252−10253.
(34) Peumans, P.; Uchida, S.; Forrest, S. R. *Nature* **2003**, *425*, 158−162.
(35) Li, A. D. Q.; Wang, W.; Wang, L.-Q. *Chem. Eur. J.* **2003**, *9*, 4594−4601.
(36) Wang, W.; Han, J. J.; Wang, L.-Q.; Li, L.-S.; Shaw, W. J.; Li, A. D. Q. *Nano Lett.* **2003**, *3*, 455−458.
(37) Wang, W.; Li, L.-S.; Helms, G.; Zhou, H.-H.; Li, A. D. Q. *J. Am. Chem. Soc.* **2003**, *125*, 1120−1121.
(38) Wang, W.; Wan, W.; Zhou, H.-H.; Niu, S.; Li, A. D. Q. *J. Am. Chem. Soc.* **2003**, *125*, 5248−5249.
(39) Gregg, B. A. *J. Phys. Chem. B* **2003**, *107*, 4688−4698.
(40) van der Boom, T.; Hayes, R. T.; Zhao, Y.; Bushard, P. J.; Weiss, E. A.; Wasielewski, M. R. *J. Am. Chem. Soc.* **2002**, *124*, 9582−9590.
(41) Asaki, M. T.; Huand, C.-P.; Garvey, D.; Zhou, J.; Kapteyn, H.; Murnane, M. M. *Opt. Lett.* **1993**, *18*, 977−979.
(42) Lukas, A. S.; Miller, S. E.; Wasielewski, M. R. *J. Phys. Chem. B* **2000**, *104*, 931−940.
(43) Greenfield, S. R.; Wasielewski, M. R. *Opt. Lett.* **1995**, *20*, 1394−1396.
(44) Greenfield, S. R.; Wasielewski, M. R. *Appl. Opt.* **1995**, *34*, 2688−2691.
(45) Giaimo, J. M.; Gusev, A. V.; Wasielewski, M. R. *J. Am. Chem. Soc.* **2002**, *124*, 8530−8531.
(46) Zang, L.; Liu, R.; Holman, M. W.; Nguyen, K. T.; Adams, D. M. *J. Am. Chem. Soc.* **2002**, *124*, 10640−10641.
(47) He, J.; Machida, S.; Kishi, H.; Horie, K.; Furukawa, H.; Yokota, R. *J. Polym. Sci. A* **2002**, *40*, 2501−2512.
(48) Kasha, M.; Rawles, H. R.; El-Bayoumi, M. A. *Pure Appl. Chem* **1965**, *11*, 371−392.
(49) Langhals, H.; Jona, W. *Angew. Chem., Int. Ed. Engl.* **1998**, *37*, 952−955.
(50) Langhals, H.; Ismael, R. *Eur. J. Org. Chem.* **1998**, 1915−1917.
(51) Würthner, F.; Thalacker, C.; Diele, S.; Tschierske, C. *Chem. Eur. J.* **2001**, *7*, 2245−2253.
(52) Saiki, Y.; Sugiura, H.; Nakamura, K.; Yamaguchi, M.; Hoshi, T.; Anzai, J. *J. Am. Chem. Soc.* **2003**, *125*, 9268−9269.
(53) Wu, J.; Watson, M. D.; Müllen, K. *Angew. Chem., Int. Ed.* **2003**, *42*, 5329−5333.
(54) *HyperChem*; Hypercube, Inc.: 1115 NW 1114th Street, Gainesville, FL 32601.
(55) Castonguay, L. A.; Rappe, A. K.; Casewit, C. J. *J. Am. Chem. Soc.* **1991**, *113*, 7177−7183.
(56) Cornell, W. D.; Cieplak, P.; Bayly, C. I.; Gould, I. R.; Kenneth, M.; Merz, J.; Ferguson, D. M.; Spellmeyer, D. C.; Fox, T.; Caldwell, J. W.; Kollman, P. A. *J. Am. Chem. Soc.* **1995**, *117*, 5179−5197.
(57) Hobza, P.; Kavelac, M.; Sponer, J.; Mejzlic, P.; Vondrasek, J. *J. Comput. Chem.* **1997**, *18*, 1136−1150.
(58) Piosik, J.; Zdunek, M.; Kapuscinski, J. *Biochem. Pharmacol.* **2002**, *63*, 635−646.
(59) Fry, A. F. *Synthetic Organic Electrochemistry*; Harper & Row: New York, 1972.
(60) Greenfield, S. R.; Svec, W. A.; Gosztola, D.; Wasielewski, M. R. *J. Am. Chem. Soc.* **1996**, *118*, 6767−6777.
(61) Weller, A. *Z. Phys. Chem.* **1982**, *133*, 93−98.
(62) Gosztola, D.; Niemczyk, M. P.; Svec, W.; Lukas, A. S.; Wasielewski, M. R. *J. Phys. Chem. A* **2000**, *104*, 6545−6551.
(63) Lukas, A. S.; Zhao, Y.; Miller, S. E.; Wasielewski, M. R. *J. Phys. Chem. B* **2002**, *106*, 1299−1306.
(64) Saigusa, H.; Lim, E. C. *Acc. Chem. Res.* **1996**, *29*, 171−178.
(65) Goldschmidt, C. R.; Ottolenghi, M. *J. Phys. Chem.* **1970**, *74*, 2041.
(66) Katoh, R.; Sinha, S.; Murata, S.; Tachiya, M. *J. Photochem. Photobiol. A* **2001**, *145*, 23−34.
(67) Kochi, J. K.; Rathore, R.; Magueres, P. L. *J. Org. Chem.* **2000**, *65*, 6826−6836.
(68) Ganesan, V.; Rosokha, S. V.; Kochi, J. K. *J. Am. Chem. Soc.* **2003**, *125*, 2559−2571.